
***fln-2* isoform-specifically regulates *Caenorhabditis elegans* health span by affecting pharyngeal function**

Received: 25 January 2026

Accepted: 5 February 2026

Published online: 11 February 2026

Cite this article as: Chang Y., Chi A., Ren Y. *et al.* *fln-2* isoform-specifically regulates *Caenorhabditis elegans* health span by affecting pharyngeal function. *Sci Rep* (2026). <https://doi.org/10.1038/s41598-026-39461-z>

Ya-Hong Chang, Ai-Qiu Chi, Yu-Chen Ren, Xue-Pan Mu, Bei-Bei Tao, Zhiyong Shao & Yi-Chun Zhu

We are providing an unedited version of this manuscript to give early access to its findings. Before final publication, the manuscript will undergo further editing. Please note there may be errors present which affect the content, and all legal disclaimers apply.

If this paper is publishing under a Transparent Peer Review model then Peer Review reports will publish with the final article.

***fln-2* isoform-specifically regulates *Caenorhabditis elegans* health span by affecting pharyngeal function**

Ya-Hong Chang^{1, #}, Ai-Qiu Chi^{1, #}, Yu-Chen Ren¹, Xue-Pan Mu¹, Bei-Bei Tao^{1, *}, Zhiyong Shao^{2, *}, Yi-Chun Zhu^{1, *}

¹ Shanghai Key Laboratory of Bioactive Small Molecules, Department of Physiology and Pathophysiology, School of Basic Medical Sciences, Fudan University Shanghai Medical College, Shanghai 200032, China

² Department of Neurosurgery, the State Key Laboratory of Medical Neurobiology and MOE Frontiers Center for Brain Science, the Institutes of Brain Science, and Zhongshan Hospital, Fudan University Shanghai, Shanghai, China

[#]: These authors contributed equally: Ya-Hong Chang, Ai-Qiu Chi

^{*}: Corresponding author:

Yi-Chun Zhu. Email: yczhu@shmu.edu.cn

Zhiyong Shao. Email: shaozy@fudan.edu.cn

Bei-Bei Tao. Email: taobeibei@fudan.edu.cn

Abstract:

Aging is regulated by both genetic and environmental factors, and *Caenorhabditis elegans* is a key model due to its conserved longevity pathways. The *fln-2* gene, encoding an ortholog of human filamin A (FLNa) with up to 27 isoforms, is known to modulate pharyngeal infection and lifespan in *C. elegans*. Still, its isoform-specific roles and mechanisms have not been fully elucidated. Here, we demonstrate that mutations specifically disrupting the longest *fln-2* isoforms (*fln-2a/e/s/t/r/u/v/w*) extend healthspan, whereas those disrupting all isoforms shorten it. The FLN-2A/E/S/T/R/U/V/W are enriched in the pharyngeal epical region, and their loss of function

results in enhanced pharyngeal grinding efficiency, reduced pharyngeal infections, decreased bacterial colonization in the intestine, and maintenance of intestinal integrity, ultimately extending lifespan. Dietary restriction has been reported to extend lifespan in multiple species, whereas the *fln-2* mutations extend lifespan without reducing food intake. These findings demonstrate the molecular mechanism by which specific *fln-2* isoforms modulate aging by enhancing pharyngeal function and reducing intestinal bacterial load, providing a new insight into FLNa's role in aging.

1. Introduction

Aging is a complex physiological process¹, often accompanied by a variety of age-related diseases, including cardiovascular diseases², cancer³, neurodegenerative diseases⁴, and even death in severe cases. Aging is modulated by genetic and environmental factors⁵. Research in model organisms has identified over 2,000 genes and 1,000 compounds that modulate lifespan⁶, demonstrating that targeted genetic interventions can significantly retard aging and elucidate its regulatory mechanisms.

Caenorhabditis elegans (*C. elegans*) is a widely used model organism for aging research due to its short lifespan and conserved genetic pathways⁷. Many aging-related genes and signaling pathways identified in *C. elegans* are conserved, including insulin/insulin-like growth factor 1 (IIS) signaling⁸, the dietary restriction (DR) pathway⁹, target of rapamycin (TOR) signaling¹⁰, the immune pathway¹¹, and the mitochondrial pathway¹². These studies made a huge contribution to understanding the regulatory mechanisms of aging.

Filamin A (FLNa), an actin-binding protein with immunoglobulin-like repeats, is integral to diverse cellular processes such as cell

proliferation, differentiation, adhesion, migration, and others^{13,14}. In *C. elegans*, the filamin ortholog is encoded by the *fln-2* gene. Previous research¹⁵ has demonstrated that the spontaneously arising *fln-2(ot611)* mutation extends lifespan by decreasing mortality due to pharyngeal infections, and this suppression of infection-related mortality in *fln-2(ot611)* mutants masks the longevity benefit typically observed in *eat-2* mutants, suggesting a shared mechanistic endpoint in mitigating pathological infection. However, the *fln-2* genomic locus exhibits considerable complexity, generating up to 27 protein isoforms through alternative splicing under the control of 15 distinct promoters¹⁶. This complexity raises several critical, unresolved questions: Which specific *fln-2* isoforms mediate the regulation of lifespan? What is the mechanistic link between *fln-2* and reduced bacterial infection? And what downstream molecular pathways are engaged?

To address these questions, we employed CRISPR-Cas9 genome editing to generate a panel of *fln-2* alleles that selectively disrupt specific groups of isoforms. Our analysis revealed that while loss-of-function mutations in *fln-2* consistently reduced pharyngeal infection, their effects on lifespan were strictly isoform-dependent. Specifically, loss-of-function mutations that specifically affect the longest isoforms (*fln-2a/e/s/t/r/u/v/w*) extend lifespan, while mutations affecting all isoforms shorten it. These findings support a model of isoform antagonism, in which the longevity benefit conferred by loss of the longest isoforms, mediated through reduced infection, is masked in pan-isoform mutants by detrimental effects stemming from the concomitant loss of shorter isoforms. Furthermore, we demonstrated that the lifespan extension resulting from loss of the longest isoforms correlates with enhanced pharyngeal grinding efficiency, leading to reduced intestinal bacterial colonization and is

associated with the activation of autophagy. Our work thus delineates an isoform-specific mechanism by which filamin modulates host-microbial interactions and organismal longevity.

2. Results

2.1 *fln-2* isoform-specifically regulates lifespan extension in *C. elegans*

During a screen for novel genetic regulators of *C. elegans* lifespan, we identified strain RB1093, which harbors a *vgln-1* deletion, that lived significantly longer. Surprisingly, we found that the causality of lifespan extension was not *vgln-1(ok1071)* but a background nonsense mutation at *Tyr739* of *fln-2* (Supplementary Fig.1). This mutant allele is genetically identical to the previously reported¹⁵ Y800* mutant allele, where a tyrosine-encoding TAC codon is converted to a stop codon (TAA). It should be noted that this difference in residue numbering comes from the update of gene annotation. According to the latest version of Wormbase, *WS296*, the mutation site encodes the 739th tyrosine of *fln-2*. As this mutation was originally identified in an EMS mutagenesis screen¹⁷ and designated *fln-2(ot611)*, we will adhere to this established nomenclature throughout the study.

To validate the impact of the *fln-2(ot611)* mutation on lifespan, we used CRISPR-Cas9 technology to generate the FDU6771 strain on a wild-type background, which carries the same *fln-2(Tyr739*)*. Consistent with previously reported findings, animals with *fln-2(ot611)* lived significantly longer at both 20°C and 25°C (Fig.1a, b). *fln-2* encodes 27 isoforms transcribed from fifteen distinct promoters¹⁶. To determine whether the longevity of *fln-2(ot611)* mutants arises from the general loss of *fln-2*, or the loss of specific isoforms, we generated *shc117* and *shc118*, which delete 1046 bp

and 1721 bp, respectively, in a region shared by all *fln-2* isoforms. To our surprise, both *shc117* and *shc118* mutants lived significantly shorter than wild-type (Fig.1c). Consistent with this, *fln-2(qx439)*, which harbors a premature stop at *Arg1199* and affects most of *fln-2* isoforms¹⁸, also lived significantly shorter (Fig.1c). Furthermore, *fln-2* RNAi targeting the shared region also reduced lifespan (Fig.1d, Supplementary Fig.2). These data suggest that the lifespan extension of *fln-2(ot611)* is most likely caused by loss of specific isoforms.

To elucidate the function of different *fln-2* isoforms, we first investigated their expression patterns. We constructed GFP transcriptional reporters for eight promoter groups (excluding the complex *fln-2g* locus, which possesses seven distinct UTRs) and generated corresponding transgenic lines (Fig.1e). The expression patterns could be generally classified into four categories: (1) *fln-2a/e/s/t/r/u/v/w*, *fln-2l/m*, and *fln-2n/o* were mainly expressed in the pharynx and hindgut; (2) *fln-2h/i*, *fln-2j/k*, and *fln-2c/d* in the hypodermis and intestine; (3) *fln-2p/q* in muscles; and (4) *fln-2f* in the intestine (Fig.1f). Notably, isoforms *j/k*, *p/q*, and *f* exhibited markedly lower expression levels, requiring higher laser power and longer exposure time for detection (Fig.1f'). These distinct expression profiles suggest that different *fln-2* isoforms likely perform specialized functions.

To examine endogenous FLN-2 expression and the effect of the *fln-2(ot611)* mutation, we analyzed the endogenous expression of the C-terminal GFP knock-in marker, which labels all *fln-2* isoforms in wild-type (a gift from Xiaocheng Wang¹⁸), and *fln-2(ot611)* mutant allele, which was generated by CRISPR (Supplementary Fig.3a). FLN-2::GFP was observed mainly in the pharynx and epidermis since the embryonic comma stage (Supplementary Fig.3b), and this pattern

persisted through postembryonic development

(Supplementary Fig.3c-f). In *fln-2(ot611)* mutants, the overall *FLN-2::GFP* signal was significantly reduced but not abolished, consistent with the hypothesis that this mutation disrupts only some specific isoforms.

The *fln-2(ot611)* mutation is predicted to affect only the longest (*fln-2a/e/s/t/r/u/v/w*) and the second longest (*fln-2h/i*) isoforms (Fig.1e), which are mainly expressed in the pharynx and hindgut based on the transgenic reporters. To validate the endogenous expression pattern of these specific isoforms, we knocked-in a GFP tag into the N-terminus of those two groups of isoforms (Fig.1g). We found that *fln-2a/e/s/t/r/u/v/w* isoforms were expressed only in the pharynx, while *fln-2h/i* were expressed in epidermis and weakly in muscles (Fig.1h). The pharyngeal signal in the *fln-2h/i* GFP strain likely results from cross-labeling of the longest isoforms, as this signal was absent in mutants specifically disrupting the longest isoform group (discussed in the following paragraph; Supplementary Fig.4). As expected, GFP expression from both reporter constructs was abolished in *fln-2(ot611)* mutants (Fig. 1h), confirming that the mutation disrupts these isoforms.

We next determined whether the lifespan extension in *fln-2(ot611)* is due to the loss of *fln-2a/e/s/t/r/u/v/w*, *fln-2h/i*, or both. We generated four additional *fln-2* mutant alleles: *shc141*, *shc142*, *shc143*, and *shc156* using the CRISPR-Cas9 approach. Among these, *shc156(Gly255*)* specifically disrupts only the longest isoforms (*fln-2a/e/s/t/r/u/v/w*), while *shc141(Gly662*)*, *shc142(Cys667*)*, and *shc143(170bp deletion)* affect both the longest and the second-longest isoforms. All four mutants displayed similar lifespan extension (Fig.1i, j), indicating loss of *fln-2a/e/s/t/r/u/v/w* isoforms is sufficient for longevity, while *fln-2h/i* either has no effect or acts in

the same pathway. We also examined the effect of *fln-2(shc156)* on the expression of *fln-2h/i* by detecting the expression of *fln-2h/i* specific GFP knock-in reporter, and found that this reporter was not affected by *fln-2(shc156)* (Supplementary Fig.4), which confirms that *fln-2(shc156)* only affects the longest group of isoforms. Collectively, these results establish that lifespan extension is specifically triggered by loss of the longest *fln-2* isoforms, setting the stage for mechanistic investigation of how these pharynx-enriched isoforms regulate aging.

2.2 *fln-2(ot611)* extends healthy lifespan

We next investigated whether the longevity conferred by *fln-2(ot611)* was accompanied by an extension of healthspan. The accumulation of the fluorescent compound lipofuscin with age is conserved in nature and can be used as a marker of health span^{19, 20}. In *C. elegans*, the accumulation of lipofuscin in the intestine can be measured using a microscope equipped with a fluorescent light source^{21, 22}. We measured the lipofuscin levels at three different timepoints (Day 1, Day 5, and Day 10), and found that the *fln-2(ot611)* mutation reduced lipofuscin levels at both middle (Day 5) and aged (Day 10) time points, but not at the Day 1 (Fig.2a, b), indicating that *fln-2(ot611)* mutants delay the rate of age-related physiological decline.

Locomotion can reflect health status and vitality²³. Therefore, we measured the locomotion ability by two indicators: body bend frequency in liquid and movement trajectory analysis. We counted the body bend frequency in liquid M9 medium and found that although there was no significant difference in the young stage (Day 2) and the middle stage (Day 5), *fln-2(ot611)* mutants bent significantly faster than the wild-type in the old stages (Day 10 and Day 15) (Fig.2c). In addition, we detected the movement trajectory of worms at Day 5 and Day 10 timepoints within 2 minutes, and found

that the movement trajectories of *fln-2(ot611)* mutants were longer than those of the wild-type (Fig. 2d).

Given that enhanced stress resistance frequently correlates with improved healthspan¹, we tested thermotolerance by exposing animals to acute high temperature stress (37°C). *fln-2(ot611)* mutants demonstrated significantly greater survival under this condition (Fig. 2e), indicating enhanced resistance. In summary, the above data collectively suggest that *fln-2(ot611)* can extend health lifespan.

2.3 The longevity effect of *fln-2(ot611)* is non-additive with *eat-2* and is independent of reduced food intake

Several genetic pathways, including mitochondrial UPR (UPR^{mt}), insulin signaling, MAPK, and dietary restriction (DR), are involved in regulating *C. elegans* lifespan. To delineate the mechanism underlying *fln-2(ot611)*-mediated longevity, we performed genetic epistasis analyses with key conserved aging pathways. We first determined whether the lifespan extension in *fln-2(ot611)* mutants is mediated by activation of UPR^{mt}, which has been shown to increase the lifespan²⁴. To address this question, we examined the expression of the UPR^{mt} reporter HSP-6::GFP in *fln-2(ot611)*, and found that the expression of this reporter was not affected (Supplementary Fig. 5). This result suggests that UPR^{mt} was not involved in the lifespan extension by *fln-2(ot611)*.

Next, we examined the insulin/insulin-like growth factor signaling (IIS) pathway. For this purpose, we analyzed the genetic interactions between *fln-2(ot611)* and *daf-2(e1370)*, and between *fln-2(ot611)* and *daf-16(mgDf50)*. *daf-2(e1370)* and *daf-16(mgDf50)* carry a reduction of function of the only insulin receptor and loss of function of the only FOXO transcription factor in *C. elegans*^{25, 26}. We found that *fln-2(ot611)* extended lifespan of both *daf-2(e1370)* and *daf-*

16(mgDf50) (Fig.3a, b, e), suggesting that *fln-2(ot611)* acts through IIS-independent signaling pathway. In addition, the nuclear localization of DAF-16, which is a key downstream transcription factor in the IIS pathway²⁷, was not affected in *fln-2(ot611)* mutants (Supplementary Fig.6). The above results collectively suggest that *fln-2(ot611)* acts independently of the IIS signaling pathway.

Furthermore, *pmk-1* is required for MAPK activation-induced lifespan extension²⁸. We asked whether *pmk-1* is required for *fln-2(ot611)* induced lifespan extension. To do this, we built *fln-2(ot611);pmk-1(km25)* double mutants and analyzed the *pmk-1*'s role in the lifespan extension of *fln-2(ot611)*. We found that the lifespan extension of *fln-2(ot611)* was not affected by the *pmk-1(km25)* mutation (Fig.3c, e), indicating that the *pmk-1* is not required for the lifespan extension of *fln-2(ot611)*.

We then tested genetic interaction with the dietary restriction (DR) pathway using the *eat-2(ad1113)* mutants, a genetic model of DR²⁹. Notably, the *fln-2(ot611)* mutation failed to extend the already long lifespan of *eat-2(ad1113)* mutants (Fig.3d, e), as previously reported¹⁵. This non-additive genetic interaction suggests that *fln-2(ot611)* and *eat-2(ad1113)* may act through overlapping or convergent mechanisms.

Since *eat-2* encodes a non- α -nicotinic acetylcholine receptor regulating food uptake through controlling pharyngeal pumping rate³⁰, we tested whether *fln-2(ot611)* similarly reduces food intake. We quantified food intake in liquid culture as described³¹ (Fig.3f), with *eat-2(ad1113)* mutants as a positive control. We found that the bacteria intake was significantly reduced in *eat-2(ad1113)* but not in *fln-2(ot611)* mutants, and the uptake was similar between *eat-2(ad1113)* and *eat-2(ad1113);fln-2(ot611)* double mutants (Fig.3g), indicating that *fln-2(ot611)* mutation does not affect the food uptake.

Consistently, *fln-2(ot611)* mutation did not affect pharyngeal pumping frequency (Fig.3h, i). These results demonstrate that while the longevity effects of *fln-2(ot611)* and *eat-2(ad1113)* are non-additive, they are mechanistically distinct: *fln-2(ot611)* does not extend lifespan by reducing food intake, which is a typical marker of DR.

Since the longevity effect of *fln-2(ot611)* is non-additive with *eat-2* and is independent of reduced food intake, we reasoned that this may be due to their high basal energy consumption. To test this, we measured their oxygen consumption rate³², as oxidative phosphorylation is the primary source of ATP production³³. We found that *fln-2(ot611)* did not change the basal respiration rate of animals, although it enhanced the maximum respiration and spare respiration of middle-aged and old animals (Supplementary Fig.7), suggesting that energy consumption is not altered in *fln-2(ot611)* mutants under normal conditions.

2.4 *fln-2(ot611)* promotes lifespan extension in an autophagy-dependent manner

Since previous studies have found that autophagy is required for dietary restriction-mediated lifespan extension³⁴, we investigated its role in the lifespan extension of *fln-2(ot611)* mutants. We first quantified the autophagy biomarker, autolysosomes³⁵, in relevant mutant strains. Both *eat-2(ad1113)* and *fln-2(ot611)* exhibited a significant increase in autolysosome levels. The double mutant allele *fln-2(ot611);eat-2(ad1113)* did not enhance the level of either single mutant (Fig.4a), indicating that they act in the same genetic pathway to promote autophagy. In addition, we quantified the nuclear localization of a key autophagy regulation transcriptional factor HLH-30^{36,37}, and found that HLH-30::GFP nuclear localization was significantly increased in the *fln-2(ot611)* mutants (Fig.4b).

To genetically establish the requirement for autophagy, we performed epistasis analyses with mutants in core autophagy genes. The lifespan extension of *fln-2(ot611)* was completely abolished in multiple autophagy-deficient backgrounds, including *atg-18(gk378)*³⁸ (Fig.4c, f), *hlh-30(tm1978)*³⁶ (Fig.4d, f), *atg-9(bp564)*³⁹ (Fig.4e, f), *unc-51(e369)* and *unc-51(e1189)*⁴⁰ (Fig.4g-i). These results demonstrate that a functional autophagy pathway is essential for *fln-2(ot611)*-mediated longevity. The non-additive increase in autophagic markers in the *fln-2(ot611); eat-2(ad1113)* double mutant aligns with their non-additive lifespan phenotype, suggesting that activation of autophagy represents a critical shared downstream node through which these genetic interventions converge to extend lifespan.

2.5 Loss of the longest *fln-2* isoforms enhances pharyngeal grinding, reduces pharyngeal infection, and limits bacterial colonization

As demonstrated, loss of the longest group of isoforms *fln-2a/e/s/t/r/u/v/w* is sufficient to induce the lifespan extension (Fig.1i, j), and these isoforms are specifically localized to the pharyngeal cuticle (Fig.1h). Staining with Congo Red, which labels the cuticle of the pharynx⁴¹, confirmed strong colocalization of the FLN-2A/E/R/S/T/U/V/W::GFP signal, particularly within the grinder structure (Fig.5a, b). Given the established links between pharyngeal function, infection, and lifespan, including the non-additive lifespan of *fln-2(ot611)* and *eat-2(ad1113)* mutants (Fig.3d, e), and the previous finding¹⁵ that *fln-2(ot611)* reduces mortality from pharyngeal infections, we speculate that changes in pharyngeal, particularly the pharyngeal cuticle and the grinder, are key to *fln-2*-mediated longevity.

To investigate whether reduced pharyngeal infection is a consistent

phenotype across different *fln-2* alleles, we quantified infection in a comprehensive panel of mutants. This analysis included wild-type N2, *fln-2(ot611)* (affecting the longest and second-longest isoforms), *fln-2(shc156)* (affecting only the longest isoforms), and *fln-2(shc117)* (a pan-isoform allele affecting all isoforms), as well as *eat-2(ad1113)* and the *fln-2(ot611); eat-2(ad1113)* double mutants. Consistent with prior finding¹⁵, all *fln-2* mutant alleles, along with *eat-2(ad1113)*, exhibited a significant reduction in pharyngeal infection incidence compared to wild-type (Fig.5c). The double mutant did not show a further reduction relative to *eat-2(ad1113)*, which parallels their non-additive lifespan phenotype (Fig.3d, e and Fig.5c). These results establish that reduced pharyngeal infection is a general consequence of *fln-2* loss-of-function, independent of isoform specificity.

Interestingly, although the pan-isoform allele *fln-2(shc117)* reduced infection (Fig.5c), its overall lifespan was significantly shortened (Fig.1c), indicating that reduced pharyngeal infection is not sufficient to extend longevity in the absence of all isoforms. This suggests that the loss of shorter isoforms, which occurs in pan-isoform mutants like *shc117*, likely imposes detrimental effects that counteract the potential lifespan benefit associated with reduced infection. In support of this possibility, microinjection of a fosmid (WRM0625cB05) harboring the shorter *fln-2* isoforms could significantly rescue the morphological defects observed in *fln-2(shc117)* mutants (Supplementary Fig.8), indicating that these shorter isoforms are crucial for normal development and viability. The main role of the grinder is grinding food bacteria⁴², and the efficiency of grinding bacteria affects the lifespan⁴³. Next, we investigated whether longevity alleles (*ot611, shc156*) enhanced the main function of the grinder. Quantification of intact GFP-labeled

bacteria in the intestine⁴⁴ revealed that while the GFP fluorescence was barely detectable in young adults (Day 1, Supplementary Fig.9), it became pronounced by Day 5 in wild-type animals. This age-dependent increase was significantly suppressed in *fln-2(ot611)* and *fln-2(shc156)* mutants (Fig.5d). These data demonstrate that the grinding efficiency is high at young stages and reduces as animals age, and *fln-2a/e/s/t/r/u/v/w(lf)* mutations promote pharyngeal grinding efficiency at the adult Day 5 stage compared to the wild-type. This reduction in intact bacterial was independently confirmed using RNA fluorescence in situ hybridization (FISH) to detect microbial colonization (Fig.5e).

All *fln-2* mutants and *eat-2(ad1113)* mutants showed significantly reduced intestinal bacterial colonization compared to wild-type. Collectively, the results indicate that loss of *fln-2* function (whether isoform-specific or pan-isoform) enhances pharyngeal grinding efficiency, thereby reducing intestinal bacteria colonization.

The intestinal barrier function is impaired with aging⁴⁵. This phenomenon is associated with the autophagy signal pathway and is alleviated in *eat-2* mutants³⁵. Previous studies have found that persistent bacterial infection leads to intestinal barrier damage⁴⁶. We therefore assessed whether *fln-2(ot611)* improves intestinal integrity using a non-absorbable blue dye, which can only stain damaged intestinal cells³⁵. Aged *fln-2(ot611)* mutants exhibited significantly improved barrier integrity compared to wild-type, and this protective effect was abolished in an *atg-18* mutant background (Fig.5f), indicating that the maintenance of intestinal barrier integrity in *fln-2(ot611)* mutants requires a functional autophagy pathway. Furthermore, given the essential role of autophagy in mediating the longevity of *fln-2* mutants, future investigations should address whether autophagy deficiency alters pharyngeal infection.

Assessing infection levels in autophagy mutant backgrounds, particularly in conjunction with *fln-2* mutations, could elucidate whether autophagy acts primarily downstream of bacterial load or also influences the initial infection process itself. This represents a promising direction for defining the precise functional interplay between microbial burden and longevity.

2.6 Lifespan extension conferred by loss of the longest *fln-2* isoforms is abolished on heat-inactivated bacteria

To assess whether the longevity of *fln-2* mutants depends on interactions with live bacteria, we performed lifespan assays using heat-killed *E. coli* OP50. When fed heat-killed bacteria, the lifespan extension of *fln-2(ot611)* mutants was completely abolished (Fig.6a). Correspondingly, intestinal bacterial colonization was undetectable in aged (Day 12) animals under this condition (Fig.6b). Furthermore, both wild-type N2 and *fln-2(ot611)* mutants displayed elevated autophagy when fed heat-killed bacteria, with no significant difference between strains (Fig.6c). Together, these data support the conclusion that the lifespan extension conferred by loss of the longest *fln-2* isoforms occurs in a context that involves interaction with live bacteria and is associated with enhanced autophagic activity.

To further clarify the relationship between isoform specificity, bacterial viability, and lifespan, we extended this analysis to the isoform-specific allele *fln-2(shc156)* and the pan-isoform allele *fln-2(shc117)*. Consistent with *fln-2(ot611)*, the lifespan extension of *fln-2(shc156)* mutants was similarly abolished on heat-killed bacteria (Fig.6d). In addition, the short-lived pan-isoform mutant *fln-2(shc117)* was significantly prolonged on heat-inactivated bacteria (Fig.6d).

Collectively, these findings lead to two main conclusions regarding

the isoform-specific function of *fln-2* in aging. First, the longevity resulting from loss of the longest *fln-2* isoforms requires live bacteria, as evidenced by the abolished lifespan extension in *fln-2(ot611)* and *fln-2(shc156)* mutants on heat-killed bacteria. This suggests their mechanism involves interaction with viable microbes, likely mediated by enhanced pharyngeal grinding that reduces infection and intestinal colonization. Second, the severe lifespan reduction in pan-isoform mutants stems from a distinct, infection-independent process. Despite reduced infectivity and colonization, the *fln-2(shc117)* mutant significantly extended lifespan on heat-killed bacteria, suggesting that the shortened lifespan was primarily due to harmful effects unrelated to bacterial infection. These effects are attributable to loss of shorter isoforms, as supported by fosmid-based morphological rescue (Supplementary Fig.8).

Thus, our data demonstrate two separable consequences of *fln-2* disruption: a mechanism by which the longest isoform-specifically regulates lifespan by reducing infection; and a pleiotropic defect resulting from the loss of the shorter isoforms, which impairs lifespan independently of infection.

3. Discussion

In this study, we demonstrate that isoform-specific disruption of *fln-2* extends healthspan and longevity in *C. elegans*. Specifically, loss of the longest *fln-2* isoforms enhances pharyngeal grinding efficiency, reduces pharyngeal infection and intestinal bacterial colonization, and extends lifespan through an autophagy-dependent mechanism that is associated with improved intestinal barrier integrity. Our analyses reveal a key isoform-specificity in lifespan regulation: loss of the longest isoforms (e.g., *shc156*, *ot611*) extends lifespan, while loss of all isoforms (e.g., *shc117*, *shc118*) or ubiquitous RNAi-

mediated knockdown shortens it (Fig.1). This opposing phenotypic outcome indicates that different *fln-2* isoforms can exert functionally antagonistic roles in aging.

The *C. elegans* filamin ortholog FLN-2 participates in diverse cellular processes, including cell migration and multivesicular body biogenesis^{13, 18}. Our work extends the foundational discovery that the spontaneous *fln-2(ot611)* allele (identical to Tyr739*, previously annotated as Y800*) extends lifespan by reducing mortality from pharyngeal infection¹⁵. We also confirmed this phenotype and further demonstrated that reduced pharyngeal infection is a consistent feature of all the longest isoforms loss-of-function alleles, including the short-lived mutant *fln-2(shc117)* (Fig.5c). This seemingly contradictory phenomenon, where reduced infection rates and shortened lifespan occur simultaneously, leads us to propose an isoform antagonistic model. We hypothesize that in pan-isoform mutants like *fln-2(shc117)*, severe detrimental effects resulting from loss of shorter, essential isoforms override the potential longevity benefit conferred by reduced infection. This interpretation is supported by the fosmid-based rescue of *shc117* morphological defects through reintroduction of shorter isoforms (Supplementary Fig.8). Although we did not perform lifespan assays on these fosmid-rescued animals due to potential overexpression effects, the morphological rescue strongly suggests that the loss of shorter isoforms underlies the developmental deficits.

Genetic interaction analysis showed non-additive lifespan effects between *fln-2(ot611)* and *eat-2(ad1113)* mutants (Fig.3d, e). While *eat-2* is a canonical genetic model of dietary restriction (DR) that acts primarily through reduced food intake³⁰, *fln-2(ot611)* does not alter pharyngeal pumping or food consumption (Fig.3g-i). Both *fln-2(ot611)* and *eat-2(ad1113)* mutants reduce pharyngeal infection

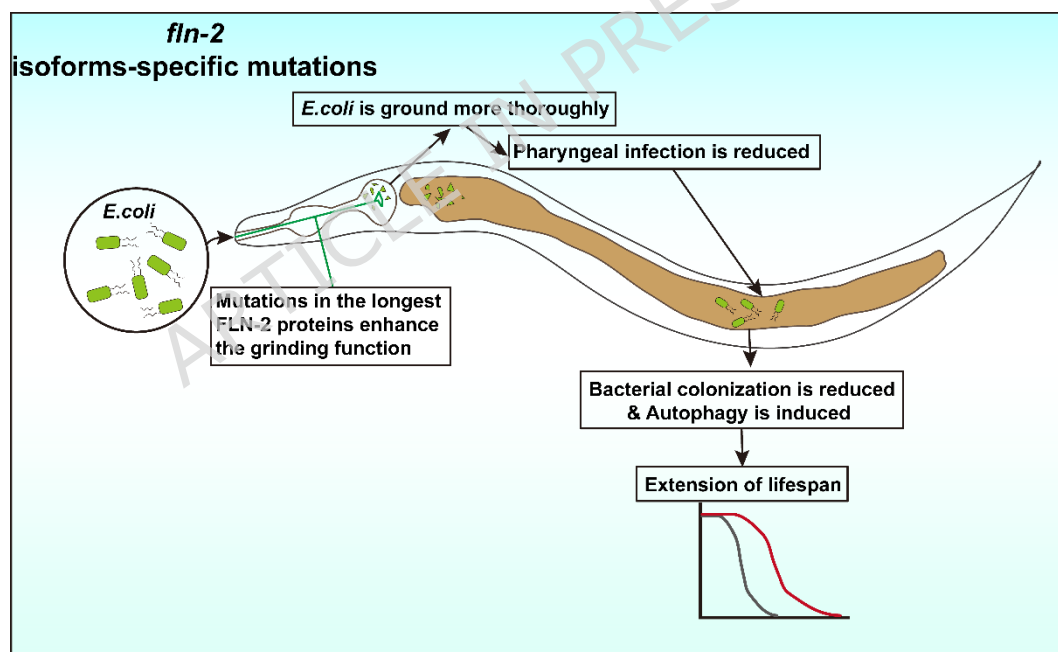
(Fig.5c), as previously described¹⁵. In addition, we found that both mutants exhibited reduced intestinal bacterial colonization and enhanced intestinal autophagy levels(Fig.5c, e). These shared changes may explain why the *fln-2(ot611)* mutation could not further extend the lifespan of the *eat-2(ad1113)* mutants. Thus, *fln-2(ot611)*-mediated longevity is mechanistically distinct from canonical dietary restriction. Instead, their genetic interaction likely results from convergence on a shared downstream outcome: both mutations significantly reduce pharyngeal infection and intestinal bacterial colonization (Fig. 5c,e), and both elevate intestinal autophagy (Fig.4a). This convergent modulation of host-microbe interaction provides a coherent explanation for their non-additive effects on lifespan.

Collectively, our results reveal a coherent longevity pathway wherein loss of the longest *fln-2* isoforms enhances pharyngeal grinding, reduces viable bacterial load, and extends lifespan in a manner that requires both live bacteria and a functional autophagy pathway. The longevity effect of *ot611* and *shc156* mutants on heat-inactivated bacteria was completely eliminated (Fig.6a, d), and their lifespan extension depended on autophagy (Fig.4), indicating that this mechanism likely works by altering interactions with live microorganisms rather than by nutritional restriction itself. The fact that the *fln-2(ot611)* mutants do not reduce food intake also supports this mechanism.

We acknowledge two primary limitations of the current study. First, while our data suggest a correlation between reduced bacterial colonization and activated intestinal autophagy upon feeding heat-inactivated bacteria, the precise causal relationship remains to be fully elucidated. Future studies utilizing bacterial genetic models with specific colonization defects, or employing temporal-resolution

analyses of autophagy induction following precise bacterial clearance, will help distinguish whether the trigger is the mere absence of live bacteria, the presence of inactivated bacterial components, or an associated nutritional shift. Second, the precise molecular functions of the large *fln-2* isoforms remain incompletely elucidated. Given the considerable size of the *fln-2* genomic locus (~30 kb), a detailed molecular-level investigation was beyond the scope of this work. Future studies employing biochemical and cell biological approaches will be essential to define how these isoforms mechanistically regulate the pharyngeal function.

Nevertheless, our research identifies *fln-2* as a critical, isoform-specific regulator that links pharyngeal function with host-microbe interactions and autophagy pathways, thereby influencing longevity.



Work model

4. Materials and methods

4.1 *C. elegans* strains and cultivation

Worms were cultured on standard nematode growth media (NGM) plates seeded with *Escherichia* OP50 bacteria⁴⁷. Unless otherwise specified, worms were usually cultured at 20°C. Bristol N2 was used as the wild-type strain in this study, and all strains used in this study are listed in Supplementary Table 1. Since the *ot611* has been found in many labs wild type, all *C. elegans* strains used in this study were sequenced at Tyr739 of the *fln-2* gene to ensure that all strains except the *fln-2(ot611)* mutants were wild-type at this locus.

4.2 Plasmids and transgenic manipulations

Plasmids were constructed with the pSM vector⁴⁸ (for transgenic plasmids) or pDD162⁴⁹ (for sgRNA plasmids) by recombination. Transgenic strains were generated by microinjecting extrachromosomal DNA arrays into the gonads of adult worms⁵⁰. DACR218 (*Punc-122::RFP*) was used as a co-injection marker. All plasmids were injected at a concentration of 20 ng/μL. In this study, the promoter sequences of each group of *fln-2* isoforms were cloned by PCR from the genome of N2 worms. Details of plasmids and primers are shown in Supplementary Table 2.

4.3 CRISPR-Cas9 editing

All mutant alleles in this study were generated using CRISPR-Cas9 editing, except for the *fln-2(syb7775)* mutant allele, which was constructed by SunyBiotech. CRISPR-Cas9 genomic editing was performed as previously described⁵¹. One or two sgRNA plasmids (50 ng/μL), one repaired template plasmid (20 ng/μL), together with three co-injected markers (*Pmyo-3::mCherry* (5 ng/μL), *Prab-3::mCherry* (15 ng/μL), and *Pmyo-2::mCherry*(5 ng/μL)), were injected into the gonads of adult worms, and the mutants were

screened in F2 progeny using PCR and DNA electrophoresis or sequencing. One repaired template plasmid is not necessary when deletion mutants are constructed. The sgRNAs were inserted into the pDD162 vector, which contained the coding sequence of Cas9. The detailed information on sgRNAs used in this study is shown in Supplementary Table 3. The repaired template plasmids contained homologous repair sequences before and after the mutation or insertion site, together with synonymous mutations in sgRNA.

4.4 RNAi (RNA interference)

Standard feeding RNA interference (RNAi) experiments were performed as previously reported⁵². Briefly, bacteria HT115 carrying the empty vector L4440 were used as a control, and HT115 carrying the same vector expressing the cDNA of interest was used for RNAi. 200 µL RNAi bacteria or control bacteria were seeded onto the RNAi plates one day before the experiment. Embryos prepared by bleaching were seeded onto the RNAi feeding plates. After 48 hours, the synchronized L4 animals were transferred to new RNAi feeding plates to start the lifespan assays.

4.5 Survival and lifespan assay

All lifespan experiments were performed on NGM plates containing *E. coli* OP50, except for those involving RNAi, where experiments were performed on *E. coli* HT115. All lifespan assays were performed at 20°C unless specified. Age-synchronized worms were acquired from gravid worms laying eggs for 2 hours on standard NGM plates. After 48 hours, about 100 synchronized L4 worms were transferred onto NGM plates seeded with *E. coli* OP50 bacteria. Worms were transferred every other day to a fresh plate containing *E. coli* OP50. For RNAi experiments, synchronized L4 worms were transferred onto RNAi feeding plates and transferred into new RNAi plates every other day. In all lifespan assays, the first day of adulthood was

considered Day 1, and the survival status of the worms was checked daily thereafter. Animals that crawled off the plate, exploded or bagged were censored. Animals that did not respond to mechanical prodding were scored as dead.

Each strain was subjected to at least three rounds of independent experiments, with each round including more than 50 worms. We used the Kaplan-Meier method to calculate the average survival rate and assessed the significance of differences in survival rates using the log-rank test. Statistical analyses were performed using GraphPad Prism (version 9.5.1). The average survival rate was calculated using the Kaplan-Meier method, and the significance of differences in survival rate was assessed using the log-rank test.

4.6 Measurement of Body length, Body bends, and Length of the trajectory

Body length

Synchronized worms on the second day of adulthood were anesthetized on 3% agarose pads with 50 mM muscimol (BACHEM, Cat: 4004216.0050). Images were acquired with an Olympus light microscope, and the length of each worm was measured using ImageJ based on the length of the scale bar. Experiments were repeated three times independently, with each time including approximately 10 animals.

Body bend frequency

For the body bends assay, synchronized L4 animals were picked onto NGM plates seeded with fresh *E. coli* OP50, and allowed to grow up at 20°C for specific time (Day 2/5/10/15). On the day of testing, the body bends of the worms in a drop of liquid M9 buffer were recorded by a camera and counted for 30 seconds. Before the measurement, worms were transferred to fresh NGM plates without *E. coli* and were allowed to crawl for 2 minutes to remove bacteria carried. The

frequency of body bends was counted after the worms were adapted to the liquid for 30 seconds. At least three biological replicates were determined for the assays, with approximately 10 worms in each experimental group.

Length of the trajectory

For the trajectory length assay, synchronized L4 animals were picked onto NGM plates seeded with fresh *E. coli* OP50, and allowed to grow up at 20°C for specific time (Day 5/10). On the day of testing, each worm was transferred to fresh NGM plates covered with *E. coli* OP50 for 2 minutes. After 2 minutes, the worm was removed, and the movement trajectory within 2 minutes was calculated by measuring the length of the scale bar.

4.7 Pharyngeal pumping rate and Food intake

Pharyngeal pumping rate

To quantify the pumping rate, at the time point of measurements (Day 1 and Day 5), worms were transferred to fresh NGM plates without *E. coli* and allowed to acclimate for 2 minutes, after which the pharyngeal pumping rate was quantified under a stereoscope within 30 seconds. Three biological replicates were determined for the assays, with approximately 10 worms in each experimental group.

Food intake

Food intake was assessed in liquid medium (S-complete medium containing 50 µg/ml Carbenicillin and 0.1 µg/ml Amphotericin B to prevent fungal or bacterial contamination). Worms were cultured in black, flat-bottomed, optically clear 96-well plates (Costar) as described previously³¹. Age-synchronized L1 worms were added to S-complete medium supplemented with antibiotics and prepared *E. coli*. Worms were diluted to about 40 worms/mL, and the *E. coli* were diluted to about 6 mg/mL using S-complete medium. The total volume per well was 150 µL. Plates were covered with sealers to

prevent evaporation, and worms were allowed to grow at 20°C for 2 days. After 2 days, 5-fluoro-2'-deoxyuridine (FUdR, Sigma, Cat: F0503) was added to each well at a final concentration of 120 μ M. Thereafter, starting from the first day of adulthood, the absorbance of each well at 600 nm (OD600) was measured using a microplate reader every 24 hours. The plate was shaken for 25 minutes before measurement and completed within 10 minutes. The number of surviving animals in each well was counted using a microscope. Finally, the food intake of each worm was calculated as follows: bacterial removal rate per well/number of worms per well.

It is important to note that this established protocol quantifies the relative depletion of a growing bacterial population. Because the bacteria replicate during the assay, the measured OD600 reflects a dynamic equilibrium between bacterial consumption by the worms and bacterial growth. Therefore, this method is suitable for comparing relative food intake between different strains under identical conditions but does not yield the absolute number of bacterial ingested by the worms.

4.8 Fluorescence microscopy and confocal imaging

Synchronized animals were anesthetized on 3% agarose pad with a drop of 50 mM muscimol for imaging. Confocal images were captured with an Andor Dragonfly Spinning Disc Confocal Microscope with 10 \times , 20 \times , 40 \times , or 60 \times objectives. GFP or DAPI was imaged with 488 or 405 nm excitation wavelength lasers, respectively. When necessary, Z-stacks of optimal range were obtained with a 0.5 μ m step size and then analyzed. Imaging of the whole animal was acquired using the stitching function. Images were processed with ImageJ (NIH) or Photoshop. The fluorescence intensity was analyzed using ImageJ (NIH).

4.9 OP50-GFP infection assays

OP50-GFP infection assays were performed as previously described¹⁵. In brief, OP50-GFP bacterial culture was cultured in LB medium supplemented with ampicillin, washed three times with antibiotic-free LB medium to remove ampicillin, and added onto NGM plates at least one day before use. Synchronized L4 animals were picked onto NGM plates seeded with fresh *E. coli* OP50-GFP, and allowed to grow up at 20°C for Day 10. On the day of testing, worms were anesthetized on 3% agarose pads with 50 mM muscimol. Next, the fluorescence distribution of the second laryngeal bulb in the pharynx was scored using a confocal microscope at 400 × magnification.

4.10 Quantitative fluorescence analysis of intestinal OP50-GFP

Synchronized L4 animals were picked onto NGM plates seeded with fresh *E. coli* OP50, and allowed to grow up at 20°C for Day 1 or Day 5. On the day of testing, worms were picked onto NGM plates seeded with fresh *E. coli* OP50-GFP for 2 hours. After 2 hours, worms were anesthetized on 3% agarose pads with 50 mM muscimol. Images were taken using an Andor Dragonfly Spinning Disc Confocal Microscope with 10× objectives. The fluorescence intensity was quantified using Image J (NIH) software.

4.11 RNA extraction, reverse transcription, and quantitative real-time PCR (qRT-PCR)

Total RNA was extracted from collected nematode samples using RNAiso Plus (Takara) and then converted to cDNA using the cDNA reverse transcription kit (TOYOBO, Cat: FSQ-201). Quantitative real-time PCR (qRT-PCR) experiments were performed using SYBR Green PCR Mix (TOYOBO, Cat: QPK-201) on the ABI 7500 system. *act-1* gene was used as an internal control. The relative expression levels

of genes were determined using the $2^{-\Delta\Delta CT}$ method and normalized to the expression of the *act-1* gene. *p*-Values were calculated using unpaired *t*-test. *p*-Values were calculated using unpaired *t*-test. The primers used for PCR were as follows (5'-3'): *act-1*, AAATCGTCCGTGACATCAAG (forward) and TCCGTCAGGAAGTTCTCGTAG (reverse); *fln-2*, CCTGAGGAAACTGGAACTTA (forward) and TCCATGTCTAGGTCGTTAAC (reverse).

4.12 Intestinal barrier function assay

Intestinal barrier function assays were performed as previously reported³⁵. Synchronized adult animals at the Day 3 or Day 12 stage were suspended for 3 hours in liquid cultures of standard OP50 bacteria mixed with blue food dye (Sigma, Cat: 861146, 5.0% wt/vol). Animals were then transferred to NGM plates seeded with OP50 bacteria for 1 hour. We used the Olympus light microscope to observe the presence or absence of blue food dye in the body cavity. For each time point, at least three independent experiments were performed, each with 20-30 animals per strain. Data were analyzed using GraphPad Prism (version 9.5.1).

4.13 RNA fluorescence in situ hybridization (FISH)

To visualize microbial colonization in *C. elegans* intestines, RNA FISH assays were performed as previously described⁵³. In brief, synchronized adult animals at the Day 12 stage were collected and then washed three times with PBST buffer, after which the animals were fixed with paraformaldehyde for 45 minutes and FISH-stained as described previously. The FISH probe used was designed for the 16S rRNA of bacteria and conjugated to Cyanine 3 (Cy3). OP50 was stained with the probe targeting the 16S rRNA sequence CAGCGAACGAGCAAGCTGC. Images were taken using an Andor Dragonfly Spinning Disc Confocal Microscope with 10 \times objectives.

The fluorescence intensity was quantified using Image J (NIH) software.

4.14 Lysotracker staining and Congo red staining

Lysotracker staining

Lysotracker staining assays were performed as previously described⁵⁴. Synchronized L4 animals were picked onto NGM plates seeded with fresh *E. coli* OP50 bacteria and allowed to lay eggs for 24 hours at 20°C. Lysotracker Red DND-99 (Invitrogen, Cat: L7528) was added at 2 µM to the NGM medium and the *E. coli* OP50 bacteria. Worms were allowed to grow up at 20°C for 3 days. Confocal images were captured with an Andor Dragonfly Spinning Disc Confocal Microscope with 10× objectives. The fluorescence intensity was quantified using Image J (NIH) software.

Congo Red staining

Congo red staining assays were performed as previously described⁴¹. 250 µL saturated distilled solution of Congo Red was added to the agar surface of NGM plates. At least 1 day later, *E. coli* OP50 was seeded onto plates and allowed to dry for at least 12 hours. Synchronized L4 animals were picked onto NGM plates containing Congo Red and allowed to grow up for 2 days at 20°C. Before imaging, animals were transferred to regular NGM plates for 2 hours to destain, after which Confocal images were captured with an Andor Dragonfly Spinning Disc Confocal Microscope with 40× objectives.

4.15 Statistical analysis

Data are presented as mean ± SEM from at least three independent biological replicates. Sample sizes (n, number of biologically independent animals or cultures) are provided in the figure legend/caption or supplementary information.

Lifespan curves were compared using the log-rank (Mantel-Cox) test, and the mean lifespan ± SEM of three repeated experiments is

presented.

For comparisons between two sets of normally distributed data, the unpair t-test is used. Comparisons among multiple groups were performed using one-way ANOVA with Tukey's multiple comparison test.

All analyses were performed in GraphPad Prism 9.5.1. Statistical significance values are indicated as follows: * $p < 0.05$; ** $p < 0.01$; *** $p < 0.001$; and n.s., not significant.

5. Data availability

All data generated or analyzed in this study are included in the article (and its supplementary information files). It can also contact the corresponding author for additional requests.

6. References

- 1 Kenyon, C. J. The genetics of ageing. *Nature* **464**, 504-512, doi:10.1038/nature08980 (2010).
- 2 Sniderman, A. D. & Furberg, C. D. Age as a modifiable risk factor for cardiovascular disease. *The Lancet* **371**, 1547-1549 (2008).
- 3 SMETANA, K. *et al.* Ageing as an Important Risk Factor for Cancer. *Anticancer Research* **36**, 5009-5017 (2016).
- 4 Hou, Y. *et al.* Ageing as a risk factor for neurodegenerative disease. *Nature reviews neurology* **15**, 565-581 (2019).
- 5 Fontana, L., Partridge, L. & Longo, V. D. Extending Healthy Life Span—From Yeast to Humans. *Science* **328**, 321-326, doi:doi:10.1126/science.1172539 (2010).
- 6 de Magalhães, J. P. *et al.* Human Ageing Genomic Resources: updates on key databases in ageing research. *Nucleic Acids Research* **52**, D900-D908, doi:10.1093/nar/gkad927 (2023).
- 7 Zhang, S., Li, F., Zhou, T., Wang, G. & Li, Z. *Caenorhabditis elegans* as a useful model for studying aging mutations. *Frontiers in*

endocrinology **11**, 554994 (2020).

8 Kenyon, C., Chang, J., Gensch, E., Rudner, A. & Tabtiang, R. A C. elegans mutant that lives twice as long as wild type. *Nature* **366**, 461-464, doi:10.1038/366461a0 (1993).

9 Lakowski, B. & Hekimi, S. The genetics of caloric restriction in *Caenorhabditis elegans*. *Proc Natl Acad Sci U S A* **95**, 13091-13096, doi:10.1073/pnas.95.22.13091 (1998).

10 Wullschleger, S., Loewith, R. & Hall, M. N. TOR signaling in growth and metabolism. *Cell* **124**, 471-484, doi:10.1016/j.cell.2006.01.016 (2006).

11 Kurz, C. L. & Tan, M. W. Regulation of aging and innate immunity in *C. elegans*. *Aging cell* **3**, 185-193 (2004).

12 Lee, S. S. *et al.* A systematic RNAi screen identifies a critical role for mitochondria in *C. elegans* longevity. *Nat Genet* **33**, 40-48, doi:10.1038/ng1056 (2003).

13 Ma, L. *et al.* FLN-2 functions in parallel to linker of nucleoskeleton and cytoskeleton complexes and CDC-42/actin pathways during P-cell nuclear migration through constricted spaces in *Caenorhabditis elegans*. *Genetics* **227**, doi:10.1093/genetics/iya071 (2024).

14 Zhou, J., Kang, X., An, H., Lv, Y. & Liu, X. The function and pathogenic mechanism of filamin A. *Gene* **784**, 145575, doi:<https://doi.org/10.1016/j.gene.2021.145575> (2021).

15 Zhao, Y., Wang, H., Poole, R. J. & Gems, D. A fln-2 mutation affects lethal pathology and lifespan in *C. elegans*. *Nat Commun* **10**, 5087, doi:10.1038/s41467-019-13062-z (2019).

16 DeMaso, C. R., Kovacevic, I., Uzun, A. & Cram, E. J. Structural and functional evaluation of *C. elegans* filamins FLN-1 and FLN-2. *PLoS One* **6**, e22428, doi:10.1371/journal.pone.0022428 (2011).

17 Sarin, S. *et al.* Analysis of multiple ethyl methanesulfonate-

mutagenized *Caenorhabditis elegans* strains by whole-genome sequencing. *Genetics* **185**, 417-430 (2010).

18 Shi, L. *et al.* Filamin FLN-2 promotes MVB biogenesis by mediating vesicle docking on the actin cytoskeleton. *Journal of Cell Biology* **221**, doi:10.1083/jcb.202201020 (2022).

19 Yin, D. Biochemical basis of lipofuscin, ceroid, and age pigment-like fluorophores. *Free Radical Biology and Medicine* **21**, 871-888, doi:[https://doi.org/10.1016/0891-5849\(96\)00175-X](https://doi.org/10.1016/0891-5849(96)00175-X) (1996).

20 Keith, S. A., Amrit, F. R. G., Ratnappan, R. & Ghazi, A. The *C. elegans* healthspan and stress-resistance assay toolkit. *Methods* **68**, 476-486, doi:<https://doi.org/10.1016/j.ymeth.2014.04.003> (2014).

21 Davis, B. O., Jr., Anderson, G. L. & Dusenbery, D. B. Total luminescence spectroscopy of fluorescence changes during aging in *Caenorhabditis elegans*. *Biochemistry* **21**, 4089-4095, doi:10.1021/bi00260a027 (1982).

22 Gerstbrein, B., Stamatas, G., Kollias, N. & Driscoll, M. In vivo spectrofluorimetry reveals endogenous biomarkers that report healthspan and dietary restriction in *Caenorhabditis elegans*. *Aging Cell* **4**, 127-137, doi:10.1111/j.1474-9726.2005.00153.x (2005).

23 Hosono, R., Sato, Y., Aizawa, S. I. & Mitsui, Y. Age-dependent changes in mobility and separation of the nematode *Caenorhabditis elegans*. *Exp Gerontol* **15**, 285-289, doi:10.1016/0531-5565(80)90032-7 (1980).

24 Shpilka, T. & Haynes, C. M. The mitochondrial UPR: mechanisms, physiological functions and implications in ageing. *Nature reviews Molecular cell biology* **19**, 109-120 (2018).

25 Gems, D. *et al.* Two Pleiotropic Classes of *daf-2* Mutation Affect Larval Arrest, Adult Behavior, Reproduction and Longevity in *Caenorhabditis elegans*. *Genetics* **150**, 129-155, doi:10.1093/genetics/150.1.129 (1998).

26 Ogg, S. *et al.* The Fork head transcription factor DAF-16 transduces insulin-like metabolic and longevity signals in *C. elegans*. *Nature* **389**, 994-999, doi:10.1038/40194 (1997).

27 Tissenbaum, H. A. DAF-16: FOXO in the Context of *C. elegans*. *Current topics in developmental biology* **127**, 1-21 (2018).

28 Kwon, G., Lee, J. & Lim, Y.-H. Dairy Propionibacterium extends the mean lifespan of *Caenorhabditis elegans* via activation of the innate immune system. *Scientific Reports* **6**, 31713, doi:10.1038/srep31713 (2016).

29 Lee, G. D. *et al.* Dietary deprivation extends lifespan in *Caenorhabditis elegans*. *Aging Cell* **5**, 515-524, doi:<https://doi.org/10.1111/j.1474-9726.2006.00241.x> (2006).

30 Avery, L. The genetics of feeding in *Caenorhabditis elegans*. *Genetics* **133**, 897-917, doi:10.1093/genetics/133.4.897 (1993).

31 Gomez-Amaro, R. L. *et al.* Measuring Food Intake and Nutrient Absorption in *Caenorhabditis elegans*. *Genetics* **200**, 443-454, doi:10.1534/genetics.115.175851 (2015).

32 Koopman, M. *et al.* A screening-based platform for the assessment of cellular respiration in *Caenorhabditis elegans*. *Nature Protocols* **11**, 1798-1816, doi:10.1038/nprot.2016.106 (2016).

33 Saraste, M. Oxidative phosphorylation at the fin de siècle. *Science* **283**, 1488-1493, doi:10.1126/science.283.5407.1488 (1999).

34 Jia, K. & Levine, B. Autophagy is required for dietary restriction-mediated life span extension in *C. elegans*. *Autophagy* **3**, 597-599 (2007).

35 Gelino, S. *et al.* Intestinal Autophagy Improves Healthspan and Longevity in *C. elegans* during Dietary Restriction. *PLoS Genet* **12**, e1006135, doi:10.1371/journal.pgen.1006135 (2016).

36 Lapierre, L. R. *et al.* The TFEB orthologue HLH-30 regulates autophagy and modulates longevity in *Caenorhabditis elegans*.

Nature Communications **4**, 2267, doi:10.1038/ncomms3267 (2013).

37 Settembre, C. *et al.* TFEB links autophagy to lysosomal biogenesis. *science* **332**, 1429-1433 (2011).

38 Erdélyi, P. *et al.* Shared developmental roles and transcriptional control of autophagy and apoptosis in *Caenorhabditis elegans*. *J Cell Sci* **124**, 1510-1518, doi:10.1242/jcs.080192 (2011).

39 Guo, B. *et al.* O-GlcNAc-modification of SNAP-29 regulates autophagosome maturation. *Nat Cell Biol* **16**, 1215-1226, doi:10.1038/ncb3066 (2014).

40 Ogura, K. *et al.* *Caenorhabditis elegans* unc-51 gene required for axonal elongation encodes a novel serine/threonine kinase. *Genes Dev* **8**, 2389-2400, doi:10.1101/gad.8.20.2389 (1994).

41 George-Raizen, J. B., Shockley, K. R., Trojanowski, N. F., Lamb, A. L. & Raizen, D. M. Dynamically-expressed prion-like proteins form a cuticle in the pharynx of *Caenorhabditis elegans*. *Biology Open* **3**, 1139-1149, doi:10.1242/bio.20147500 (2014).

42 Straud, S., Lee, I., Song, B., Avery, L. & You, Y.-J. The jaw of the worm: GTPase-activating protein EAT-17 regulates grinder formation in *Caenorhabditis elegans*. *Genetics* **195**, 115-125 (2013).

43 Portal-Celhay, C., Bradley, E. R. & Blaser, M. J. Control of intestinal bacterial proliferation in regulation of lifespan in *Caenorhabditis elegans*. *BMC Microbiol* **12**, 49, doi:10.1186/1471-2180-12-49 (2012).

44 Kumar, S. *et al.* Lifespan Extension in *C. elegans* Caused by Bacterial Colonization of the Intestine and Subsequent Activation of an Innate Immune Response. *Developmental Cell* **49**, 100-117.e106, doi:10.1016/j.devcel.2019.03.010 (2019).

45 Salazar, A. M., Aparicio, R., Clark, R. I., Rera, M. & Walker, D. W. Intestinal barrier dysfunction: an evolutionarily conserved hallmark of aging. *Disease models & mechanisms* **16**, dmm049969 (2023).

46 Ma, Y.-C. *et al.* YAP in epithelium senses gut barrier loss to deploy defenses against pathogens. *PLoS pathogens* **16**, e1008766 (2020).

47 Brenner, S. The genetics of *Caenorhabditis elegans*. *Genetics* **77**, 71-94 (1974).

48 Shen, K. & Bargmann, C. I. The immunoglobulin superfamily protein SYG-1 determines the location of specific synapses in *C. elegans*. *Cell* **112**, 619-630, doi:10.1016/s0092-8674(03)00113-2 (2003).

49 Dickinson, D. J., Ward, J. D., Reiner, D. J. & Goldstein, B. Engineering the *Caenorhabditis elegans* genome using Cas9-triggered homologous recombination. *Nat Methods* **10**, 1028-1034, doi:10.1038/nmeth.2641 (2013).

50 Berkowitz, L. A., Knight, A. L., Caldwell, G. A. & Caldwell, K. A. Generation of stable transgenic *C. elegans* using microinjection. *J Vis Exp*, doi:10.3791/833 (2008).

51 Friedland, A. E. *et al.* Heritable genome editing in *C. elegans* via a CRISPR-Cas9 system. *Nat Methods* **10**, 741-743, doi:10.1038/nmeth.2532 (2013).

52 Kamath, R. S. & Ahringer, J. Genome-wide RNAi screening in *Caenorhabditis elegans*. *Methods* **30**, 313-321, doi:[https://doi.org/10.1016/S1046-2023\(03\)00050-1](https://doi.org/10.1016/S1046-2023(03)00050-1) (2003).

53 Rivera, D. E., Lažetić, V., Troemel, E. R. & Luallen, R. J. RNA Fluorescence in situ Hybridization (FISH) to Visualize Microbial Colonization and Infection in *Caenorhabditis elegans* Intestines. *J Vis Exp*, doi:10.3791/63980 (2022).

54 Lapierre, L. R., Gelino, S., Meléndez, A. & Hansen, M. Autophagy and lipid metabolism coordinately modulate life span in germline-less *C. elegans*. *Current Biology* **21**, 1507-1514 (2011).

55 Albertson, D. G. & Thomson, J. N. The pharynx of *Caenorhabditis elegans*. *Philos Trans R Soc Lond B Biol Sci* **275**, 299-325,

doi:10.1098/rstb.1976.0085 (1976).

7. Acknowledgments

We thank Xiaochen Wang for kindly supplying the XW16577 and XW20193 strains. Some strains were obtained from the *Caenorhabditis* Genetics Center (CGC).

8. Funding

This research was supported by the Ministry of Science and Technology, People's Republic of China (2021YFA0909300 and 2022YFE0205400), the National Natural Science Foundation of China (32371227, 32370877, 32170828 and 31830042), the Noncommunicable Chronic Diseases-National Science and Technology Major Project (2023ZD0503203), and the Macau Science and Technology Development Fund (FDCT) (0007/2019/AKP to Yichun Zhu).

9. Author information

Authors and Affiliations

Shanghai Key Laboratory of Bioactive Small Molecules, Department of Physiology and Pathophysiology, School of Basic Medical Sciences, Fudan University Shanghai Medical College, Shanghai 200032, China

Ya-Hong Chang, Ai-Qiu Chi¹, Yu-Chen Ren, Xue-Pan Mu, Bei-Bei Tao¹, Yi-Chun Zhu

Department of Neurosurgery, the State Key Laboratory of Medical Neurobiology and MOE Frontiers Center for Brain Science, the Institutes of Brain Science, and Zhongshan Hospital, Fudan University Shanghai, Shanghai, China

Zhiyong Shao

Contributions

Author contributions include the following: Y.C., Z.S., and Y.Z. conceived and designed the project. Y.C., A.C., Y.R., and X.M. performed the experiments. Z.S., Y.C., and A.C. analyzed the experimental data and interpreted the experimental results. Y.C., Z.S., and Y.Z. wrote the manuscript. B.T. revised the manuscript. All authors have read and agreed to the published version of the manuscript.

Corresponding author

Correspondence to Yi-Chun Zhu.

10. Ethics declarations

Competing interests

The authors declare no competing interests.

11. Figures and figure legends

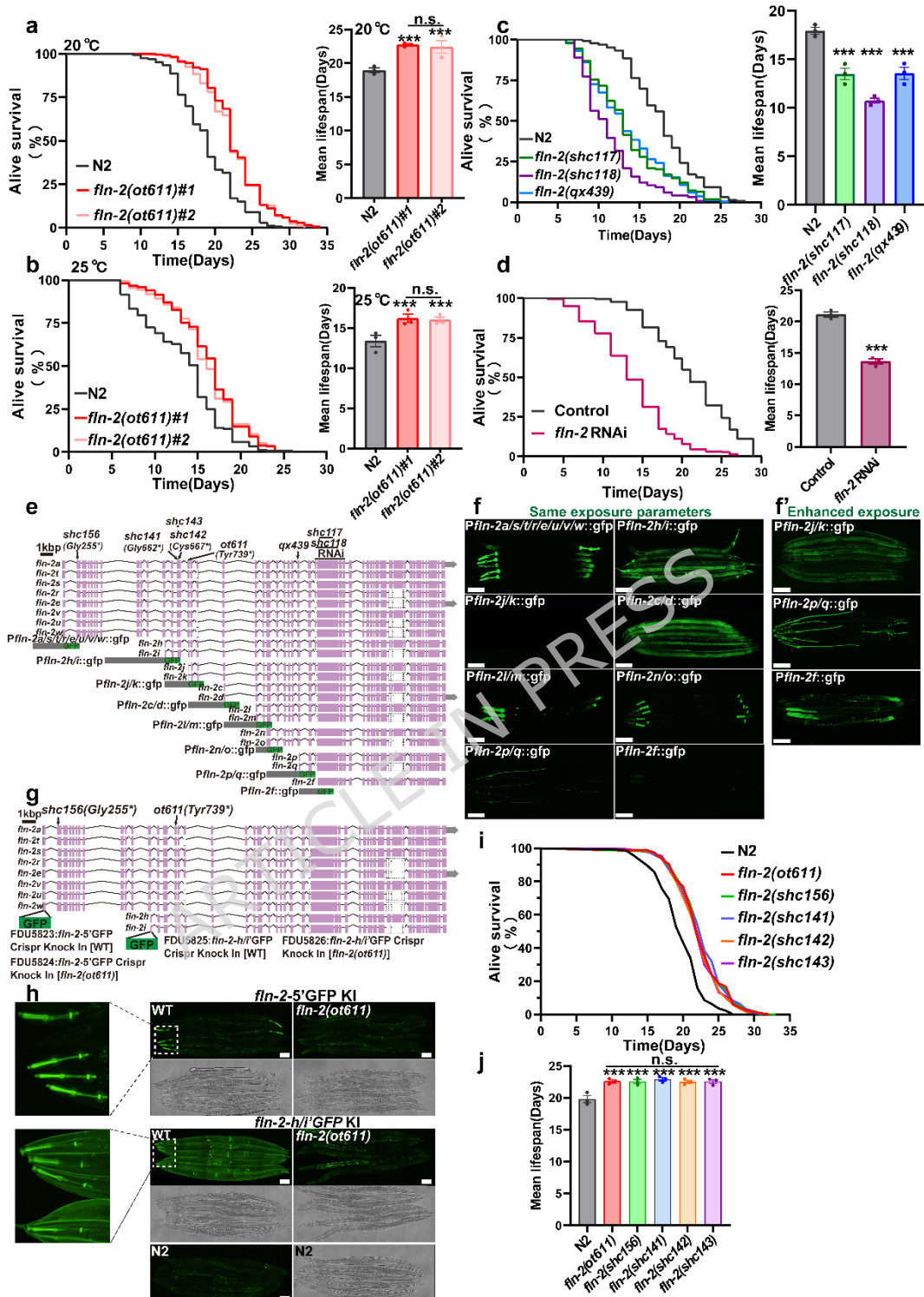


Fig.1 *fln-2* isoform-specifically extends the lifespan of *C. elegans*.

a, b Lifespan curves and mean lifespans of wild-type N2 and *fln-2(ot611)* mutants at 20°C (a) or 25°C (b). See Supplementary Table 4 for details. **c**

Lifespan curves and mean lifespans of wild-type N2 and *shc117/shc118* mutants affecting all *fln-2* isoforms. See Supplementary Table 5 for details. **d** Lifespan curves and mean lifespans of N2 worms treated with control (HT115) or *fln-2* RNAi. See Supplementary Table 5 for details. **e** A schematic diagram of reporter constructs for 21 CDS-encoding isoforms of the *fln-2* gene. The sequence information is retrieved from the Wormbase database (<https://wormbase.org/>). Purple boxes and lines indicate exons and introns, respectively. Gray boxes indicate untranslated regions, and the dotted box represents the missing part of this isoform. The scale bar in the diagram is 100 bp. The deletion region of mutant alleles *shc117*, *shc118* and *shc143* is indicated with a line segment, while the mutation sites of the mutant alleles *ot611*, *shc141*, *shc142*, *shc156* and *qx439* are indicated by arrows. **f** Representative confocal images of the *Pfln-2*(different groups of isoforms)::gfp of L4 animals under the same exposure parameters. **f'** Representative confocal images of the *Pfln-2(j/k)::gfp*, the *Pfln-2(p/q)::gfp*, the *Pfln-2(f)::gfp* of L4 animals under enhanced exposure parameters. Scale bar is 100 μ m and applied to the rest of the images unless specified. **g** Schematic diagram of knocking in a GFP encoding sequence into the 5' site of the longest or second-longest groups of *fln-2* isoforms. **h** Representative confocal images of the longest and second-longest groups of FLN-2 proteins of Day 1 animals. **i, j** Lifespan curves (**i**) and mean lifespans (**j**) of N2, *shc156* mutants that affect only the longest isoforms, and *shc141/shc14/shc143/ot611* mutants that affect the longest and second-longest isoforms. See Supplementary Table 6 for details. All lifespan experiments were repeated three times independently. Summary of mean lifespans is shown as mean lifespan \pm SEM. *p*-Values were determined using the log-rank test. ****p* < 0.001; and n.s., not significant.

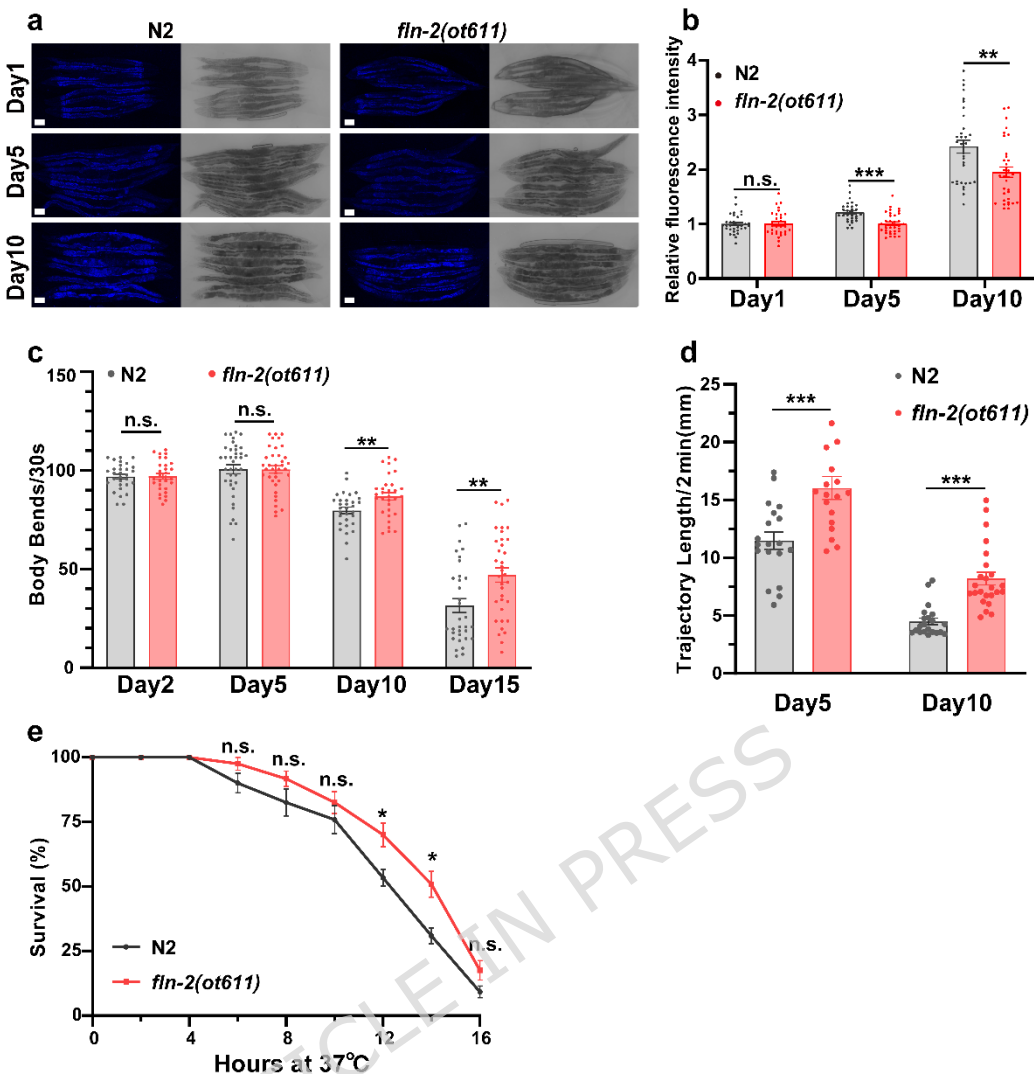


Fig.2 *fln-2 (ot611)* promotes the healthspan of *C. elegans*.

a, b Representative fluorescence images of lipofuscin (**a**) and quantification of the intensity (**b**) of wild-type N2 or *fln-2(ot611)* mutants at Day 1/5/10. The scale bar is 100 μ m. **c** Body bends frequency of wild-type N2 and *fln-2(ot611)* mutants in liquid at Day 2/5/10/15. **d** The length of the trajectory of wild-type N2 and *fln-2(ot611)* mutants at Day 5/10. **e** Survival curves of Day 3 wild-type N2 and *fln-2(ot611)* animals at 37°C. All experiments were repeated three times independently, and all data are presented as means \pm SEM. Differences between two groups were determined by the unpair *t*-test. * p < 0.05; ** p < 0.01; *** p < 0.001; and n.s., not significant.

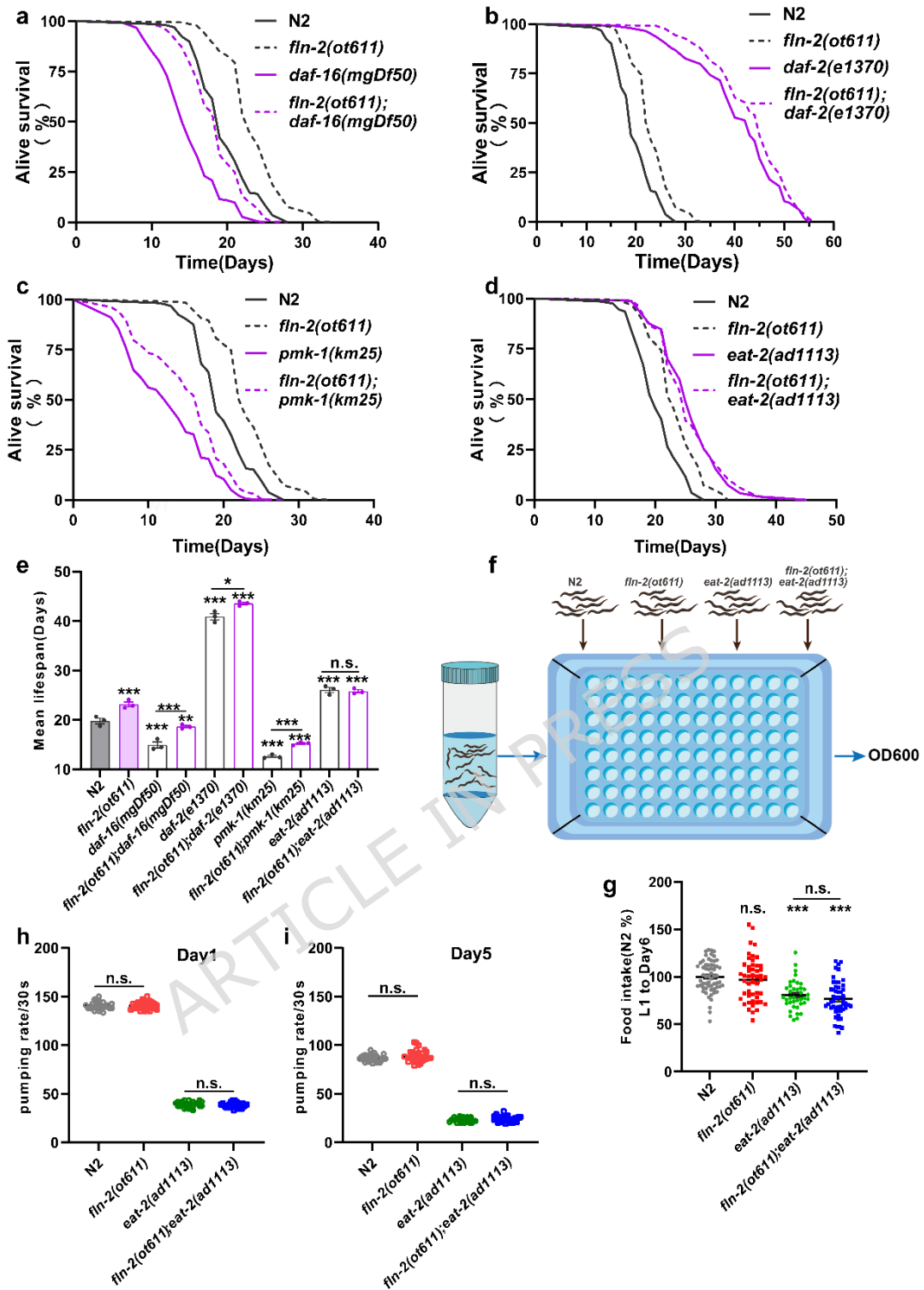


Fig.3 The lifespan extension of *fln-2(ot611)* mutants is associated with dietary restriction pathways without affecting their food intake.

a-d Lifespan curves of wild-type N2, *fln-2(ot611)*, *daf-16(mgDf50)* (a), *daf-2(e1370)* (b), *pmk-1(km25)* (c), *eat-2(ad1113)* (d) single mutants, and *fln-2(ot611);daf-16(mgDf50)* (a), *fln-2(ot611);daf-2(e1370)* (b), *fln-2(ot611);pmk-1(km25)* (c), *fln-2(ot611);eat-2(ad1113)* (d) double mutants. The double mutants show a lifespan extension similar to the single mutants.

1(km25) (**c**), *fln-2(ot611);eat-2(ad1113)* (**d**) double mutants. **e** Summary of mean lifespans. Data are presented as mean lifespan \pm SEM. *p*-Values were determined using the log-rank test. $*p < 0.05$; $**p < 0.01$; $***p < 0.001$; and n.s., not significant. See Supplementary Table 7 for details. **f** Food intake of worms was assessed in liquid medium. **g** Relative food intake of wild-type N2 and *fln-2(ot611)* mutants. **h, i** Pharyngeal pumping frequency of wild-type N2 and *fln-2(ot611)* mutants at Day 1 (**h**) or Day 5 (**i**) stages. Data in (**g-i**) are shown as means \pm SEM. Differences between multiple groups were determined using one-way ANOVA with Tukey's multiple comparison test. $***p < 0.001$; and n.s., not significant.

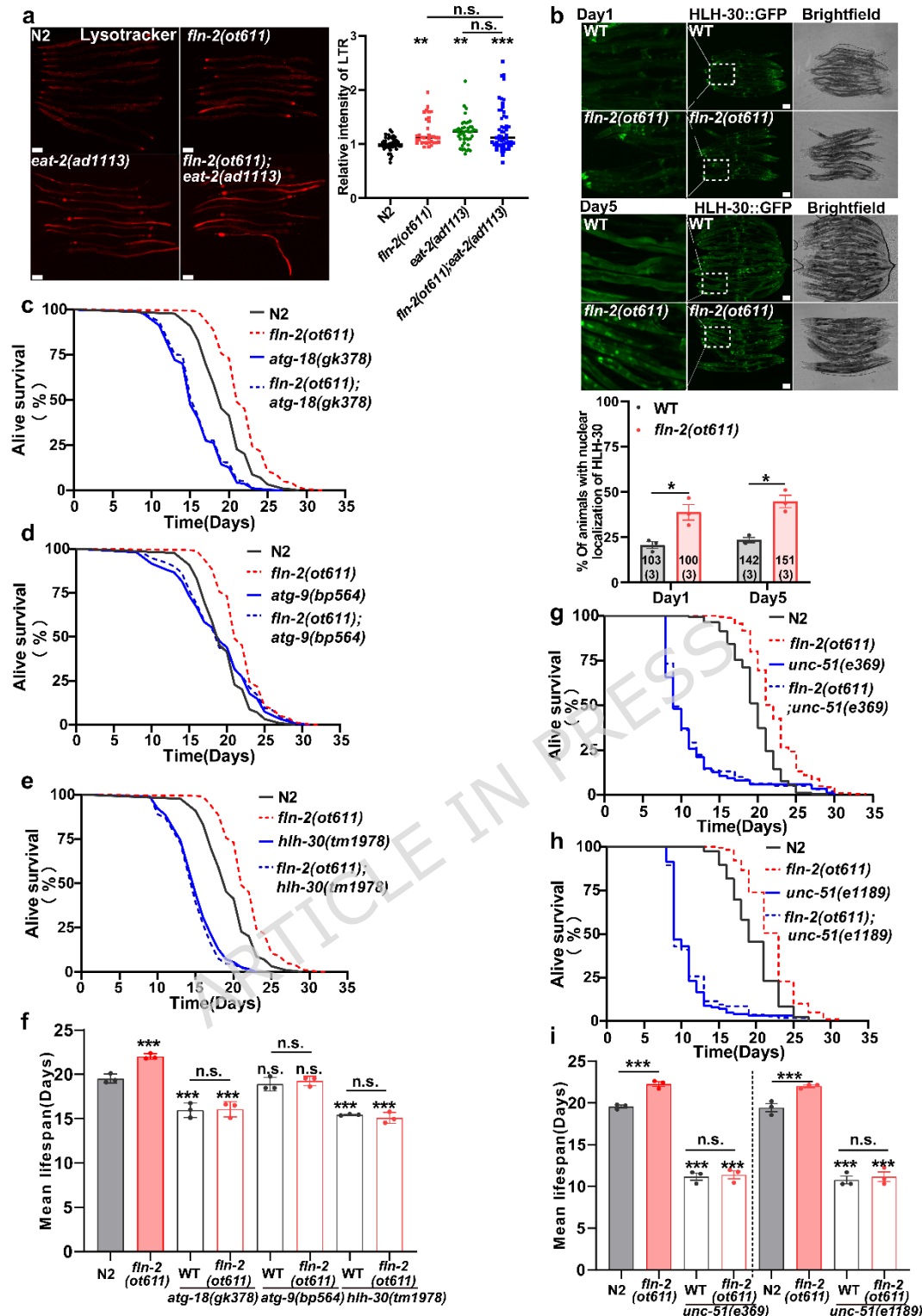


Fig.4 The lifespan extension of *fln-2(ot611)* mutants is associated with autophagy signaling.

a Representative fluorescence images of acidic lysosome staining of Day 3 wild-type N2, *fln-2(ot611)*, *eat-2(ad1113)*, and *fln-2(ot611);eat-2(ad1113)* double mutants. The right side shows the relative fluorescence intensity. **b**

Representative fluorescence images of HLH-30::GFP of wild-type N2 and *fln-2(ot611)* mutants at Day 1 or Day 5 stage. The side below shows the percentage of animals with HLH-30 in the nuclei of intestinal cells. The specific information is marked below the bar graph in the form of N(n), where N represents the total number and n represents the number of experiments. The data are shown as means \pm SEM. *p*-Values were determined by the unpair *t*-test. **c-i** Lifespan curves of wild-type N2, *fln-2(ot611)*, *atg-18(gk378)* (**c**), *atg-9(bp564)* (**d**), *hlh-30(tm1978)* (**e**), *unc-51(e369)* (**g**), *unc-51(e1189)* (**h**) single mutants, and *fln-2(ot611);atg-18(gk378)* (**c**), *fln-2(ot611);atg-9(bp564)* (**d**), *fln-2(ot611);hlh-30(tm1978)* (**e**), *fln-2(ot611);unc-51(e369)* (**g**), *fln-2(ot611);unc-51(e1189)* (**h**) double mutants. **f, i** Summary of mean lifespans. Data are presented as mean lifespan \pm SEM. The experiments were repeated three times independently, and *p*-Values were determined using the log-rank test. See Supplementary Table 8, 9 for details. **p* < 0.05; ****p* < 0.001; and n.s., not significant.

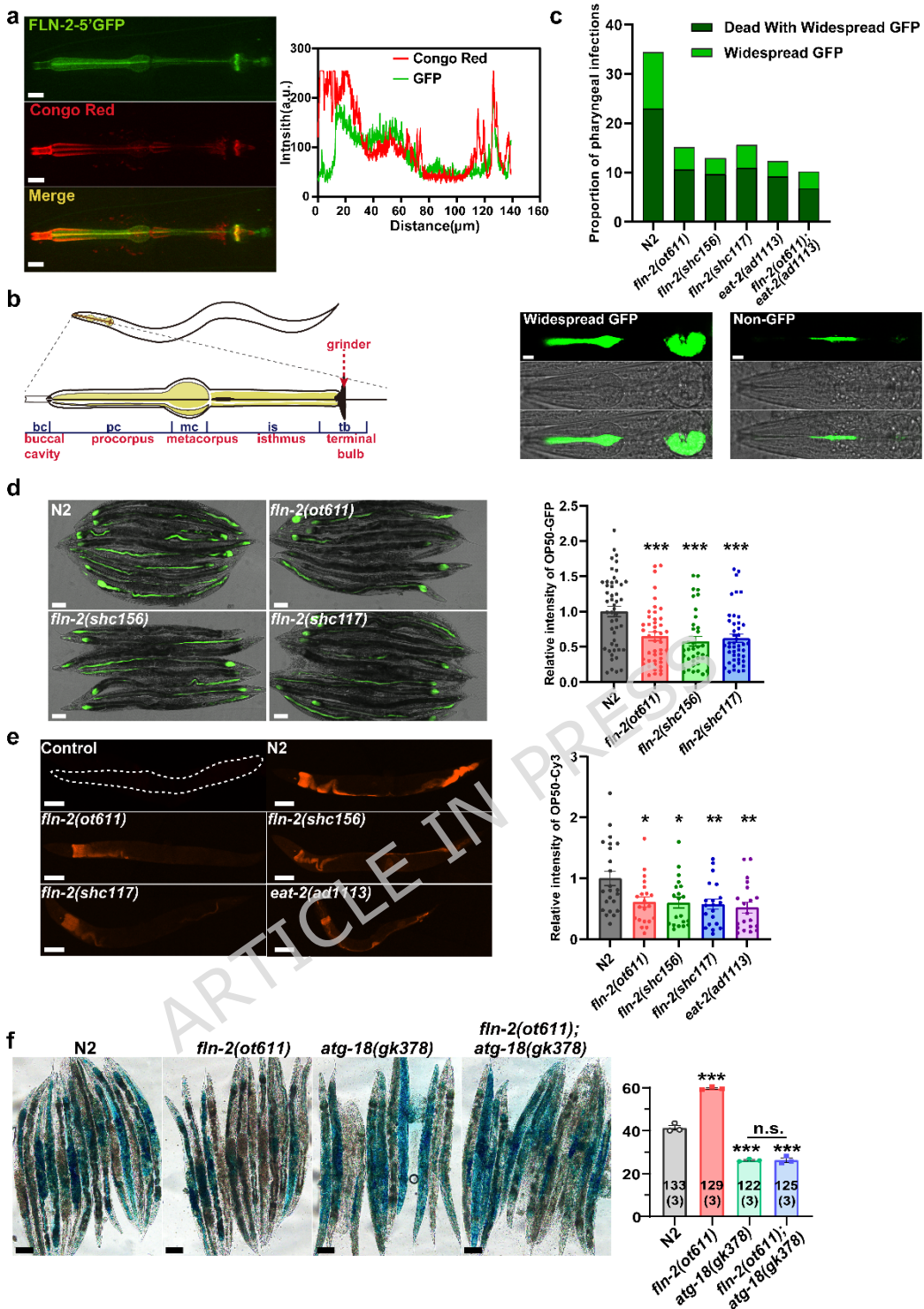


Fig.5 fin-2a/e/s/t/r/u/v/w(lf) mutations enhance pharyngeal grinding and digestion of bacteria, reducing pharyngeal infections and intestinal bacterial colonization.

a Fluorescence images and colocalization analysis of GFP-tagged the longest FLN-2 proteins and Congo red staining for marking the pharyngeal cuticle. **b** Schematic diagram of the *C. elegans* pharynx⁵⁵. The functional divisions of the

pharynx are shown from left to right: the buccal cavity, procorpus, metacorpus, isthmus, and terminal bulb. **c** Scoring of pharyngeal widespread infection of wild-type N2, *fln-2(ot611)*, *fln-2(shc156)*, *fln-2(shc117)*, *eat-2(ad1113)*, and *fln-2(ot611);eat-2(ad1113)* mutants fed with *E. coli* expressing GFP using fluorescence microscopy. Animals used in this experiment were at the Day 10 stage. The right side shows examples of pharyngeal infection with OP50-GFP *E. coli*. **d** Fluorescence images of wild-type N2, *fln-2(ot611)*, *fln-2(shc156)*, and *fln-2(shc117)* mutants after being transferred to plates seeded with *E. coli* expressing GFP at the Day 5 stage, and the relative fluorescence intensity of uncultured bacteria in the intestine. **e** Representative fluorescence images of FISH staining of wild-type N2, *fln-2(ot611)*, *fln-2(shc156)*, *fln-2(shc117)*, and *eat-2(ad1113)* at Day 12 stage. The right side shows the relative fluorescence intensity. The scale bar is 100 μ m and experiments were repeated three times independently. *p*-Values were determined using one-way ANOVA with Tukey's multiple comparison test. ***p* < 0.01; ****p* < 0.001; and n.s., not significant.

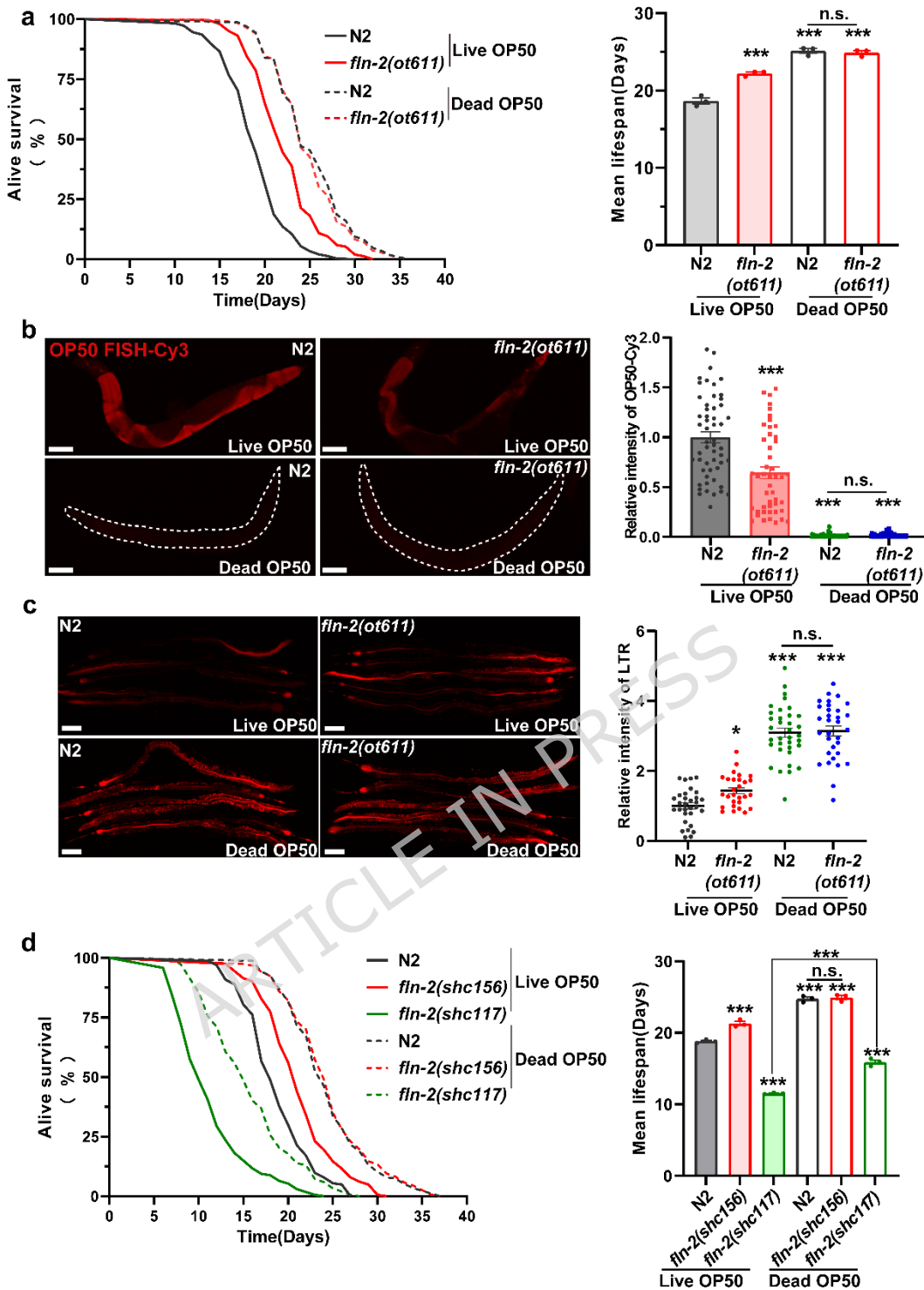


Fig.6 The longevity of the *fln-2a/e/s/t/r/u/v/w(lf)* mutants disappeared in heat-inactivated bacteria.

a Survival curves of wild-type N2 and *fln-2(ot611)* fed with normal *E. coli* or heat-killed *E. coli*, respectively. The right side shows the summary of mean lifespans. Data are presented as mean lifespan \pm SEM. See Supplementary Table 10 for details.

b Representative fluorescence images of FISH staining of *OP50* (Cy3) and *N2* (red). The bottom panels show the corresponding fluorescence images of the *OP50* cell lysate. Scale bars are shown in the bottom left of each image.

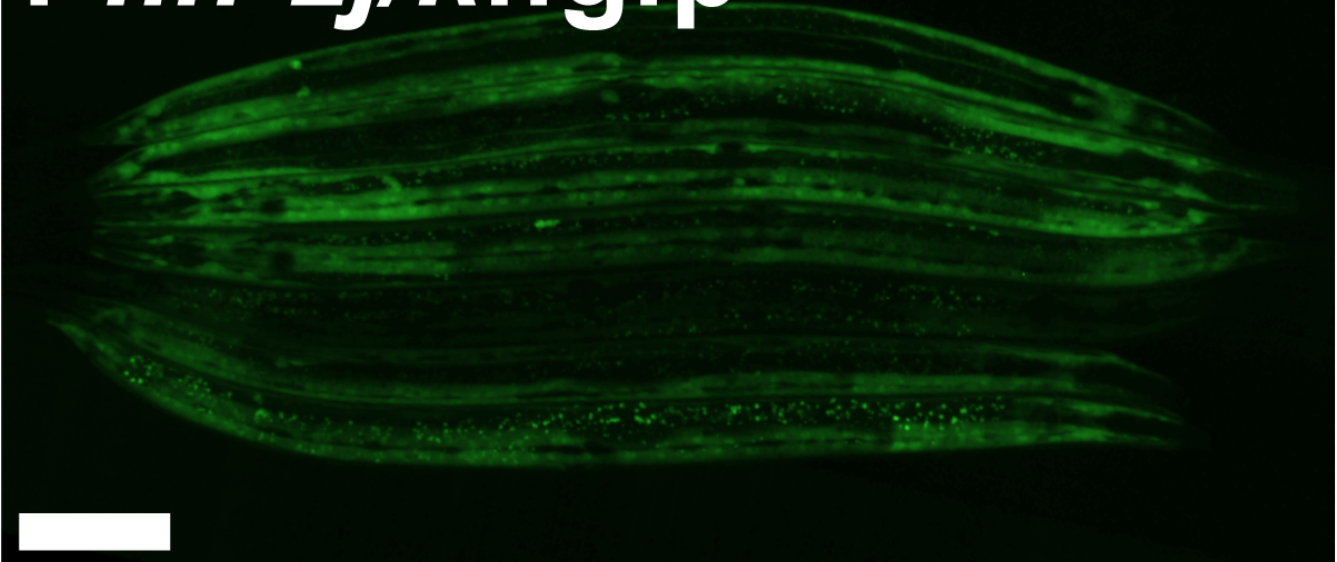
c Representative fluorescence images of FISH staining of *OP50* (Cy3) and *N2* (red). The bottom panels show the corresponding fluorescence images of the *OP50* cell lysate. Scale bars are shown in the bottom left of each image.

d Survival curves of wild-type N2 and *fln-2(shc156)* and *fln-2(shc117)* fed with normal *E. coli* or heat-killed *E. coli*, respectively. The right side shows the summary of mean lifespans. Data are presented as mean lifespan \pm SEM. See Supplementary Table 10 for details.

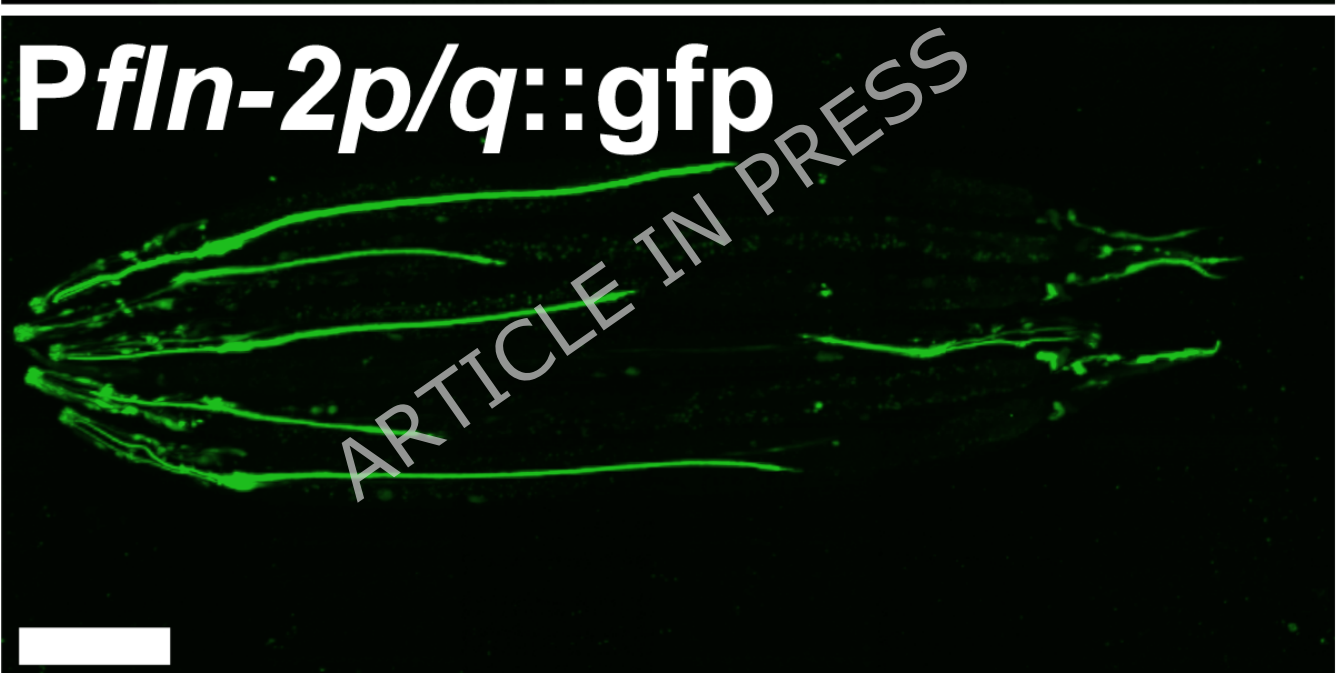
wild-type N2 and *fln-2(ot611)* animals fed with normal or heat-killed *E. coli* at the Day 12 stage. The right side shows the relative fluorescence intensity. **c** Representative fluorescence images of acidic lysosome staining of Day 3 wild-type N2 and *fln-2(ot611)* fed with normal or heat-killed *E. coli*, respectively. **d** Survival curves of wild-type N2, *fln-2(shc156)*, and *fln-2(shc117)* animals fed with normal or heat-killed *E. coli*, respectively. The right side shows the summary of mean lifespans. Data are presented as mean lifespan \pm SEM. See Supplementary Table 11 for details. The right side shows the relative fluorescence intensity. *p*-Values in **(a, d)** were determined using the log-rank test, *** p <0.001; and n.s., not significant. *p*-Values in **(b, c)** were determined using one-way ANOVA with Tukey's multiple comparison test. * p <0.05; *** p <0.001; and n.s., not significant.

f'

Enhanced exposure *Pfln-2j/k::gfp*



Pfln-2p/q::gfp



Pfln-2f::gfp

